A unifying model for pyroclastic surge genesis and pyroclastic flow fluidization

Karim Kelfoun, Valentin Gueugneau

Geophysical Research Letters
RESEARCH LETTER
10.1029/2021GL096517

A unifying model for pyroclastic surge genesis and pyroclastic flow fluidization

Karim Kelfoun, Valentin Gueugneau

Université Clermont Auvergne, CNRS, IRD, OPGC, Laboratoire Magmas et Volcans, F-63000 Clermont-Ferrand, France.
Corresponding author: karim.kelfoun@uca.fr

Key Points: (1) We present a coherent model for the high-fluidity of small-volume pyroclastic flows and for the genesis of ash-cloud surges
(2) Conclusions are drawn from field observations at Merapi volcano, laboratory experiments and numerical models
(3) The movement of the rock fragments on the steepest slopes of the volcano both creates the pyroclastic surge and induces large runouts

Abstract

Pyroclastic density currents are hot and fast ground−hugging mixtures of volcanic fragments and gases, which represent a major threat to people living near to explosive volcanoes. Mechanisms causing the separation into the concentrated (the pyroclastic flow) and dilute (the pyroclastic surge) layers, as well as the mechanism causing their remarkably high mobility are still unclear. Here we present a conceptual model based on field observations of lava dome collapses, laboratory experiments, and numerical modelling that unifies these mechanisms. Our model shows that they are caused by the fall of fine volcanic particles onto steep, irregular topography. The ambient air entrapped during the fall both creates the pyroclastic surge through elutriation and induces high fluidity in the pyroclastic flow by increasing its pore pressure. Our conclusion reveals the importance of topography in the destructive capacity of pyroclastic density currents.

Plain Language Summary

Pyroclastic density currents are hot and fast ground−hugging mixtures of volcanic fragments and gases, which represent a major threat. These gravity-driven currents are characterized by a remarkably high mobility and are composed of two components: (1) a high concentration layer, the pyroclastic flow, which is formed of ashes and lava blocks and is confined to valleys, and (2) a dilute upper layer, the pyroclastic surge, which is formed of small particles suspended in hot turbulent gases and can be thick enough to overflow the valleys and destroy surrounding areas. However, mechanisms causing the separation into the concentrated and dilute layers, as well as the mechanism causing their high mobility are still unclear. Here we present a conceptual model based on field observations, laboratory experiments, and numerical modelling that unifies these mechanisms. Our model shows that they are caused by the fall of fine volcanic particles onto steep, irregular topography. The ambient air entrapped during the fall both induces high fluidity in the pyroclastic flow by increasing the air pressure in its pores and creates the pyroclastic surge through expulsion of the finest particles. Our conclusion reveals the importance of topography in the destructive capacity of pyroclastic density currents.

1. Introduction

Understanding the complex dynamics of pyroclastic density currents (PDCs) is an enduring quest in volcanology (Sparks et al., 1978; Druitt, 1998; Branney & Kokelaar, 2002; Dufek 2016, Lube et al. 2019, 2020). Based on the characteristics of PDC deposits in the field, volcanologists have distinguished two regimes in PDCs, which are now viewed as endmembers (Burgisser & Bergantz, 2002; Lube et al, 2020; Valentine, 2020): the high particle concentration regime of pyroclastic flows, and the low particle concentration regime of pyroclastic surges. Nevertheless, and despite recent large-scale experiments (Lube et al, 2015, 2019; Bréard et al., 2016; Bréard & Lube, 2017) and multiphase numerical simulations (Esposti Ongaro et al, 2012; Bréard et al.

2018; Valentine & Sweeney, 2018; Valentine, 2020), our knowledge of the processes leading to the marked non-uniformity of PDCs and to their high fluidity is still incomplete.

Here we focus on small-volume PDCs, caused by lava dome collapses. A remarkable characteristic of these PDCs, besides their high recurrence, is their high mobility and the fluid-like behavior of the pyroclastic flow. For volumes usually smaller than ~10^7 m^3, these flows reach several kilometers, sometimes more than ten kilometers (Komorowski et al., 2013; Cronin et al., 2013) from their source, destroying everything in their path. The role of the insterstitial gas, atmospheric and/or volcanic, is often invoked to explain this extreme fluidity. Overpressure of this interstitial gas generates a pressure gradient between the flow's upper surface and its interior, which counteracts the particles' weight and consequently the frictions in the flow (Druitt et al. 2007; Montserrat et al 2016; Roche; 2012; Lube et al., 2019). However, the origin of this gas is still debated, and the following hypotheses have been put forward: volcanic gases released by lava pore breakage (Sato et al. 1992), atmospheric gases incorporated at the flow front (Mc Taggart, 1960), gas trapped during column collapse (Sparks & Wilson, 1976 ; Wilson, 1980) or during sedimentation of the flow particles (Druitt, 1995), gas from the intergranular pore-space (Lube et al. 2019) or gas trapped in a rough substratum (Chedeville et Roche, 2014, 2018). The genesis of the ash-cloud surge has been explained by gas-release processes that would elutriate the fine particles from the pyroclastic flow (Wilson, 1980), by the expulsion of gas and fines at the impact site of collapsing mixtures (Sweeney & Valentine, 2017; Valentine, 2020), by particle fragmentation (Fujii and Nakada, 1999), by the entrainment of ambient air due to its thermal expansion (Sparks, 1976) or to the turbulence created by the flow displacement (Denlinger, 1987; Dufek 2016).

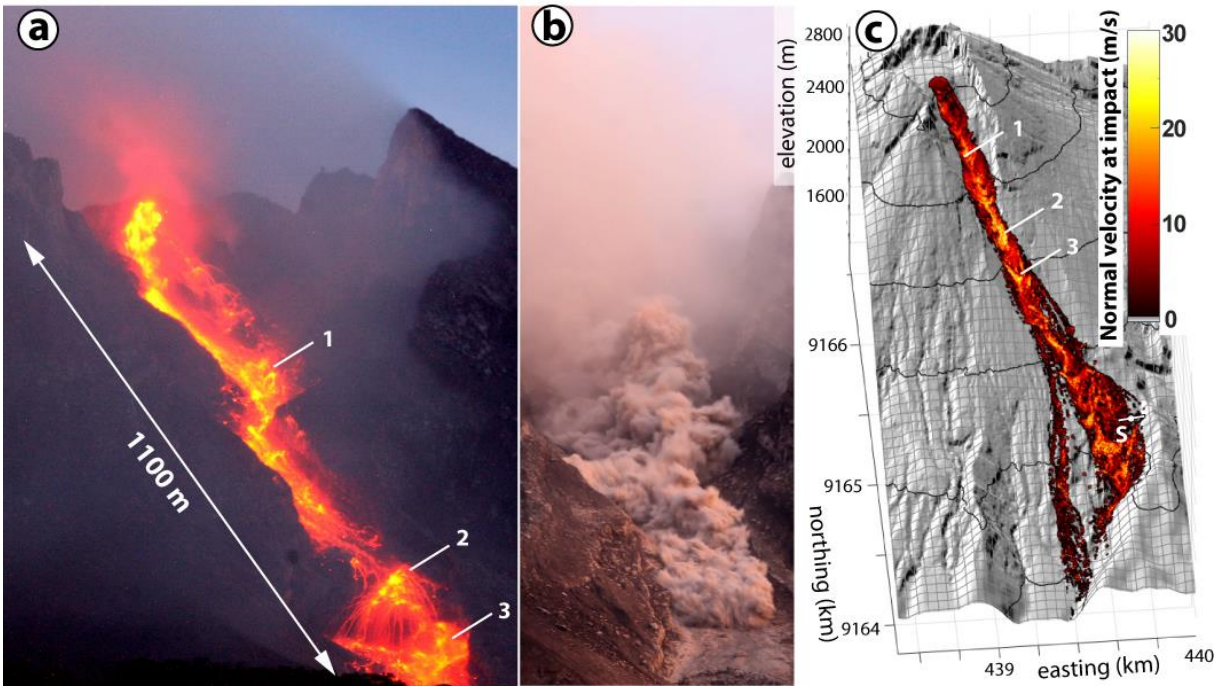

Figure 1. Pyroclastic flow and surge from a dome collapse at Merapi volcano. (a) Long exposure image (night shot) showing the block trajectories through the surge and locations where larger blocks break into finer blocks and ash (yellow color). (b) The pyroclastic surge during daytime, which hides the flow. (c) Simulation of the impact velocities of the blocks down the slope (see section 3). Numbers in white indicate the reference locations in photograph (a). S is the source of the flow in Fig. 5 and for the flow model.

Our incomplete understanding of the links between the different processes at work during PDC emplacement is mostly due to the difficulty of observing PDC formation. Recent long-term (2014-2022) and continuous observation of PDCs caused by lava dome collapses at Merapi volcano in Indonesia (Kelfoun et al, 2021) shows that both the flow and the surge begin by blocks of hot, brittle lava that bounce and break on the steepest slopes of the volcano (Fig. 1). Our study is based on the idea that the two main characteristics of small volume PDCs, i.e., the high mobility and the surge formation, can both be caused by this repeated upward/downward movement of the fragmented lava over steep volcanic slopes.

2. A fluidization-elutriation process related to particle fall

We designed an experimental setup (Text S1) to investigate the mechanisms that occur when pyroclastic flow particles leave the ground after a shock or a topographic bump, then fall back down and hit the ground. Either natural pyroclastic material or glass beads of various diameters (38 μm, 77 μm, 550 μm or 2 mm) were put in a tank that was oscillated vertically. More than 150 experiments (Table S1) were carried out to test variations in the granular material, its temperature (between 50°C and 450°C), and the vibration properties (frequencies 1 to 13 Hz, amplitudes 1 and 2 cm).

The ascent phases firstly accelerated the particles upwards. When the upward tank velocity decreased, the inertia and particle interactions caused the gas-particle mixture to expand and ingest air. For large glass beads (ϕ = 550 μm and 2 mm), the particles collided and the air had little influence on their dynamics. However, for small glass beads (ϕ = 38 and 77 μm) and natural PDC material, the particles interacted strongly with the air. Moreover, with the natural polydisperse material, oscillations formed fingers of high particle concentration separated by zones of low particle concentration (Fig. 2a). The width of each finger (about 2 to 4 mm) seems to have been controlled by the largest particle at its head. Their height depended on the initial particle velocities given, in the experiments, by the amplitude and the frequency of the tank and it can be predicted from a ballistic model of the largest particles (Eq. 12 and 13 of Text S2 and Fig. S3). When the fingers fell back down due to gravity, their velocity measured by the displacements of the finger structures was close to the fall velocity of the largest isolated particles. All the particles, regardless of their size, followed the same movement (Fig. S3), and the relatively unchanged morphologies of the fingers during the fall suggest that the particle concentration in the fingers remained approximately constant except at their base where two key processes were observed to be operated simultaneously;

(i) Firstly, the air trapped in the concentrated bed formed by settling was compressed, creating an elevated pore pressure that induced a fluid-like behavior of the concentrated bed with surface waves, air bubbles and convective displacements below, as already observed for granular shaking (Pak & Behringer, 1994; Zamankan, 2012; Matsusaka et al., 2013), granular fall experiments (Fries et al., 2021) and numerical modeling (Sweeney & Valentine, 2017; Valentine, 2020).

(ii) Secondly, the upward movement of air expelled from the collapsing fingers caused the finest particles to be elutriated and form an ash cloud above the oscillating tank (Fig 2b and S3). Each oscillation supplied new material to the cloud, increasing its thickness and density (higher light absorption observed), up to a point at which the plume partially or totally collapsed to form a density current that flowed into our experimental channel (Fig. 2c). The cloud formed at each oscillation was about half the height of the fingers (Fig. 2b). At the scale of the experiments, the temperature

(from ambient to 500°C) had no observable role in the finger dynamics but it controlled the cloud density and, consequently, the proportion of particles that entered the density current or the plume.

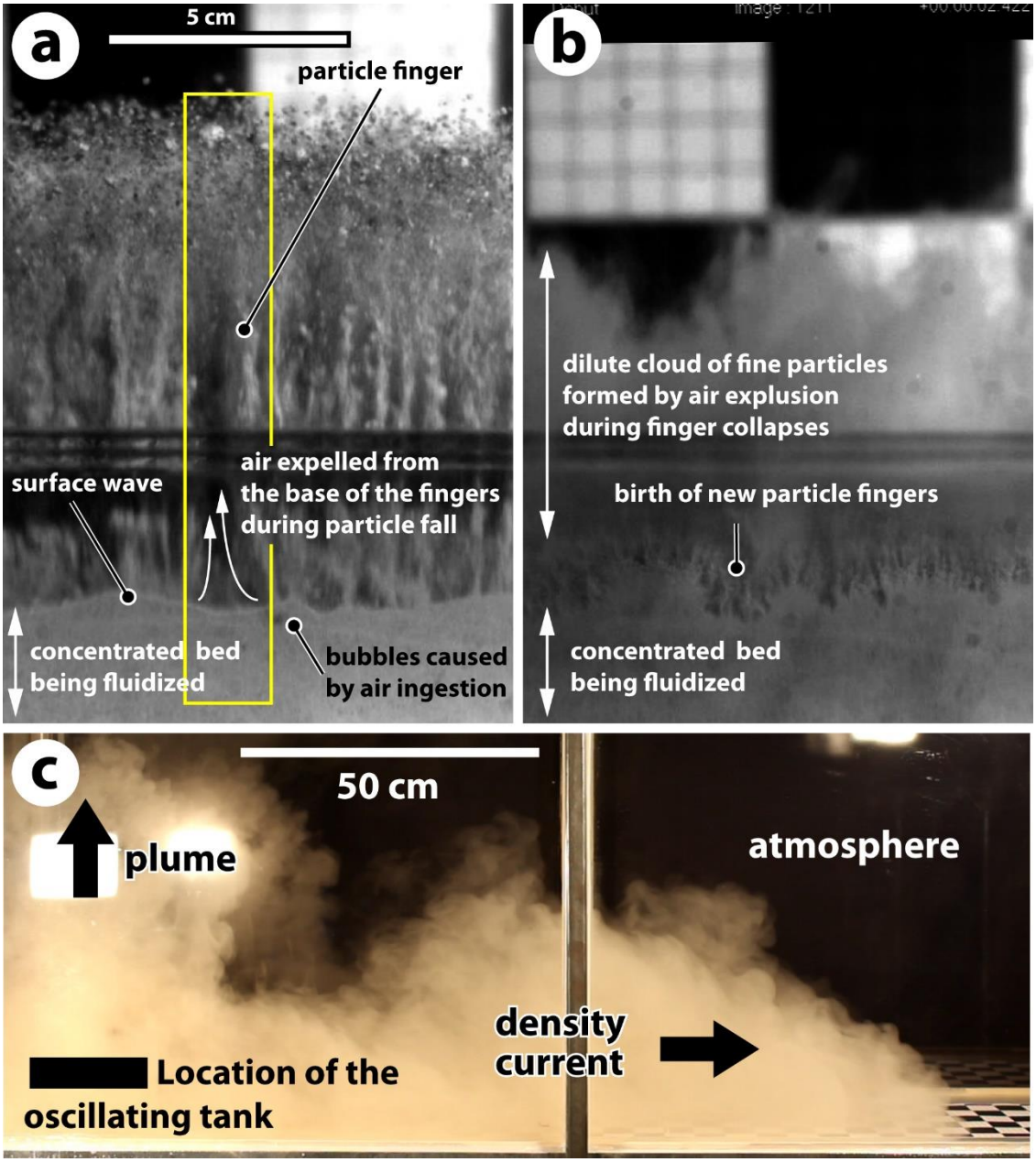

Figure 2. Experimental setup with natural PDC particles (Nescher ignimbrite, see Text S1). Natural particles, temperature 100°C, amplitude 2 cm, frequency 12 Hz. (a) High-speed camera image of the first stage of the dilute cloud genesis with the fluidization of the lower concentrated part and the particle jets (t = 200 ms). (b) Dilute cloud formed by air expulsion during jet collapses (t = 260 ms). Subsequent jets increase the thickness and density of the cloud. (c) Experimental density current and ash cloud plume at t = 6 s (42 oscillations).

.

The upward velocity u_c of air between the fingers was controlled by volume conservation (i.e. mass conservation in incompressible conditions) and depended on the fall velocity u_f of the fingers, the particle volume fractions of the fingers ϕ_f, the concentrated bed ϕ_b and the cloud ϕ_c,

and on the ratio of the basal surfaces of the fingers S_f and the cloud S_c (Fig. S4 and Text S1 for demonstration):

$$u_c = \left(\frac{S_f}{S_c}\right)\left(\frac{\phi_b - \phi_f}{\phi_b - \phi_c}\right) \times u_f \quad (1)$$

Particles are carried upwards if the velocity of the rising gas u_c is greater than their fall velocity u_p, given by (Sparks et al., 1997; Bonnadona et al., 1998):

$$u_c > u_p = \sqrt{\frac{4(\rho_p - \rho_a)gd}{3C_d\rho_a}} \quad (2)$$

where ρ_p is the particle density, ρ_a the air density, g the gravity and C_d the particle drag coefficient. All the particles with a diameter smaller than d were carried upwards. In the experiment presented in Fig. 2, which used natural PDC material, the mean fall velocity of the finger relative to the tank was 1.4 m/s. The ratio of the finger surface to the cloud surface, S_f / S_c ranged between 0.5 and 1, ϕ_b was about 60%, ϕ_f deduced from the height of the fingers and the thickness of their deposit was about 4% and ϕ_c was <<1%. This gave a maximum theoretical diameter of between 30 and 120 μm, consistent with morphometric analysis of the particles settled from the gravity current in our experiments (PSD distribution of Fig. 3).

3. Fluidization-elutriation on volcanic topography

The laboratory experiments show that, at their scale, the repeating fall of particles, containing fines, reproduces two fundamental characteristics of PDCs: a fluidization of a basal concentrated bed, and its elutriation to form an associated ash-cloud. On a real volcano, the question is what the conditions of this genesis are, i.e. where does a mixture of gas and particles fall to the ground from a great enough height to entrain atmospheric air and form a cloud of particles ? To address this question, we calculated the trajectories of the largest blocks of a pyroclastic flow on real topography. The blocks can slide, they can leave the ground and follow a ballistic trajectory, and they can bounce on the ground. Details of the simulation, equations and links to numerical codes used are available in Text S2. We chose Merapi volcano, in Indonesia, for our study, as one of its valleys has been affected by recent and well-observed PDCs (Gendol valley, SE flank, in 2006, 2010, 2019 and 2021; Charbonnier & Gertisser, 2008; Charbonnier et al. 2013; Komorowski et al., 2013). The starting area of the trajectories was defined by the front of the lava dome relating to the largest collapses in March 2019 (Kelfoun et al, 2021) and in July 2021.

Results of the modelling show that two mechanisms allow a block to leave the ground and to fall back down: following deflection by a collision and following a passage over a topographic bump. In both cases, the block velocity down the slope must be sufficiently high. According to the model, this is entirely dependent on the slope of the volcano. Bouncing is rapidly damped down by inelastic collisions, but a steep slope means that even a bounce with a null vertical component can reach a relatively high elevation and subsequently fall several meters. Moreover, on slopes steeper than the friction angle of the rocks (about 30°), the block accelerates by sliding once on the ground until it bounces again. On gentler slopes, the block decelerates and rapidly comes to a stop after a few bounces (Fig. S7).

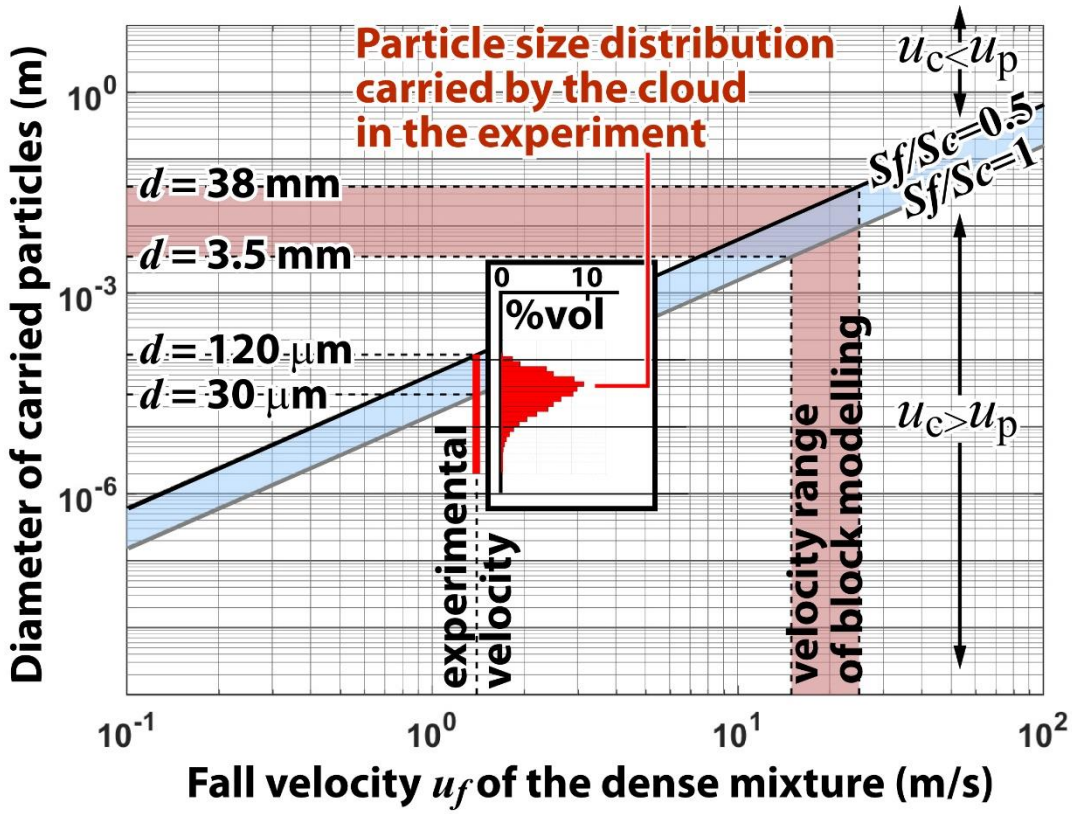

Figure 3. Maximal diameter of the particles carried upwards according to the finger settling velocity (Eq. 1 and 2). The diagonal blue area gives the range of maximal particle sizes according to the range of the ratio of the surface of the fingers to the surface of the dilute cloud. All particles with diameters lying below the blue area can be carried by the cloud. The red histogram gives the size distribution of the particles carried upward by the experimental cloud and the red line shows the experimental conditions (settling velocity and range of carried particle sizes). The pink strip shows the highest fall velocities computed by the block modelling (see below) and the related size of transported particles according to Eqs. 1 and 2.

The model shows that impacts at velocities higher than 15−25 m/s occur along the 2.4 km of the summit cone (Fig. 1c). Based on Eqs. 1 and 2, and assuming that the mechanism of air ingestion and expulsion found in our experiments also occurs in the field, a cloud with a minimal thickness of 30 m and particles larger than 3.5 mm could be created (Fig. 3). Even though the geometries of the falling particle mixture and the rising cloud are significantly different in the field compared to our experiments, the air must be expulsed due to volume conservation and an upward velocity of the expulsed air of only 20% of the fall velocity is capable of transporting the millimeter-sized particles of pyroclastic surges.

4. Fluidized flows and long-runout

The conclusions of the block modelling and the laboratory experiments suggest that the strongest surge genesis and fluidization of the concentrated current by particle bouncing are found on all slopes steeper than ≈ 30°. Below this slope angle, however, the phenomenon is absent.

Given that the mechanism appears to be efficient only on the steeper slopes, a question arises: does this mechanism allow a concentrated current to flow over more than 10 km on relatively gentle slopes, as is observed in reality? In order to answer this, we have used a new version of the numerical model VolcFlow that simulates the emplacement of fluidized granular flows (Kelfoun and Druitt, 2005; Gueugneau et al., 2017). The flow is considered to follow a

Voellmy-Salm friction rheology, often used for natural granular flows (Hungr and Evans, 1996; De'Michieli Vitturi et al., 2019; Patra et al, 2020; Peruzzetto et al., 2020; Gueugneau et al., 2021), which combines frictional and turbulent/collisional models. The pore pressure of gases influences the frictional term of the Voellmy-Salm law and the retarding stress **T** of the flow is given by:

$$\mathbf{T} = \frac{\mathbf{u}}{\sqrt{u_x^2 + u_y^2}} \left[\left(\rho g h - P_b + P_s \right) \tan\varphi + \frac{\rho g}{\xi} \left(u_x^2 + u_y^2 \right) \right] \quad (3)$$

where $\mathbf{u} = [u_x, u_y]$ is the flow velocity along the local slope, ρ the mean flow density, h its thickness, P_b and P_s the gas pressure at the base and surface of the flow, φ the Coulomb friction angle, ξ the Voellmy turbulence coefficient and g gravity. At the foot of the summit cone (source located in Fig. 1c and 4a, slope ≈ 30°), where the blocks cease to bounce, the flow is considered to be entirely fluidized, with an initial thickness h_0 imposed over a given duration Δt_0. Several hypotheses (initial thickness and velocity, gas diffusivity, flow able to expand or not by gas pressure, etc.) were explored and, details of the simulations and codes used are available in Text S3.

Simulations show that the flow duration T and the distance L reached by the flow front are controlled by the diffusion time scale $\frac{h^2}{D}$ where h is the mean thickness and D the gas diffusivity of the flow. Whatever the options chosen for the simulations, long runouts observed in the field (i.e. 5.9 and 15.5 km for the 2006 and 2010 Merapi eruptions respectively; Charbonnier and Gertisser, 2008; Komorowski et al., 2013) can be reached for relatively thick flows (e.g. initial thickness h_0 > 10 m for a null initial velocity, mean thickness h > 4 m) and for a diffusivity of about 0.01 $m^2 s^{-1}$ (Fig. 4a), which is compatible with natural thicknesses and material properties (Druitt et al., 2007; Lube et al, 2011; Montserrat et al. 2012; Roche 2012; Charbonnier et al. 2013). For a given valley width, the volume rate imposes the flow thickness, which strongly influences the runout: a flow will more easily achieve a long-runout in a valley than on flat topography. A minimum flow duration and, consequently, a minimum volume are required to maintain the flow thickness and to reach long runouts. However, after a given duration (>100 s in the simulations of Fig. 4b), the conditions at the rear of the flow no longer influence the front, which is then controlled by its own defluidisation, and the extra volume (>2.23×10^6 m^3 for the red curve of Fig. 4b) does not change the runout. Instead, the extra volume fills the valley and overflows laterally, encroaching on the interfluves. Overflow induces flow spreading and thinning and, consequently, an increase in pressure gradient and flow re-fluidization. The threat for the surrounding population is that re-fluidized flows may accelerate suddenly and spread out laterally at high velocity on the interfluves.

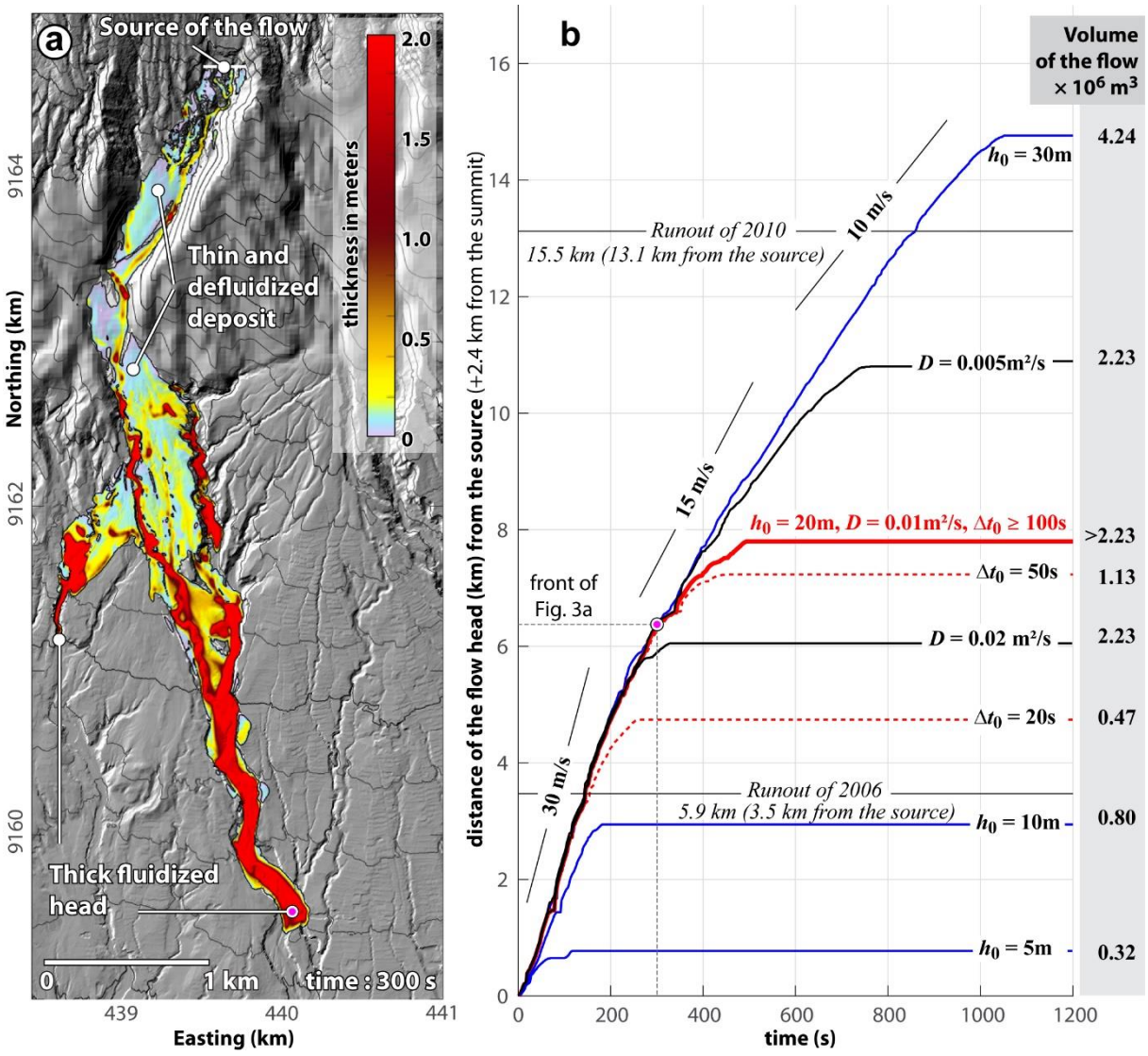

Figure 4. Simulation of a pyroclastic flow in the Gendol valley of Merapi volcano for non-expanded flows with a null initial velocity. (a) map of the thicknesses at t = 300 s for h_0=20m, D=0.01 m²/s and a genesis duration Δt_0 = 100 s. (b) Distances reached by the flow front with time using various values of h_0, D and Δt_0. Reference curve is shown in red (h_0=20m, D=0.01 m²/s, Δt_0=100s). For Δt_0>100, the front dynamics are independent of the value of Δt_0. The figures marked on the other curves indicate the parameter that is different with respect to the reference conditions. The two horizontal lines, at 5.9 and 15.5 km, indicate the runouts of the 2006 and the 2010 eruptions. The values to the right give the volumes of the simulated pyroclastic flows.

5. A coherent model of PDC genesis and emplacement

Our field observations, experiments and numerical modelling lead to a coherent and global dynamical model of small-volume PDC genesis and emplacement (Fig. 5), dominated by a cyclic mechanism of ejection/compaction of the pyroclastic material over steep, rough volcanic slopes. After the collapse of a lava dome, a highly concentrated avalanche forms and its hot lava fragments roll, slide and bounce on the steepest slopes of the volcano and break into fine ash through these successive shocks. The high velocity reached allows the rock fragments to detach from the ground, from some cm to tens of meters, by experiencing innumerable shocks and on jumping over topographic bumps. This causes a dilatation of the concentrated avalanche and ingestion of air. When the flow falls back to the ground, it compacts itself and ejects part of the entrapped air toward the flow surface, expelling the smallest particles. This key

mechanism causes both the fluidization of the flow and the formation of a mixture of fine ash and gas. Fine ash accumulates progressively above the flow and forms an ash-cloud that is denser than the atmosphere. This fluidization-elutriation process continues as long as the slope angle allows it and is stronger on the steepest slopes. On lower and generally gentler slopes, the bounce height is reduced. However, if a cliff is present, the fluidization-elutriation process starts again, causing an increase in the mobility of the flow as well as the density of the surge. Our model can thus explain the relationship that has already been described between topography and sudden surge destructiveness (Nakada and Fujii, 1993; Kelfoun et al., 2000).

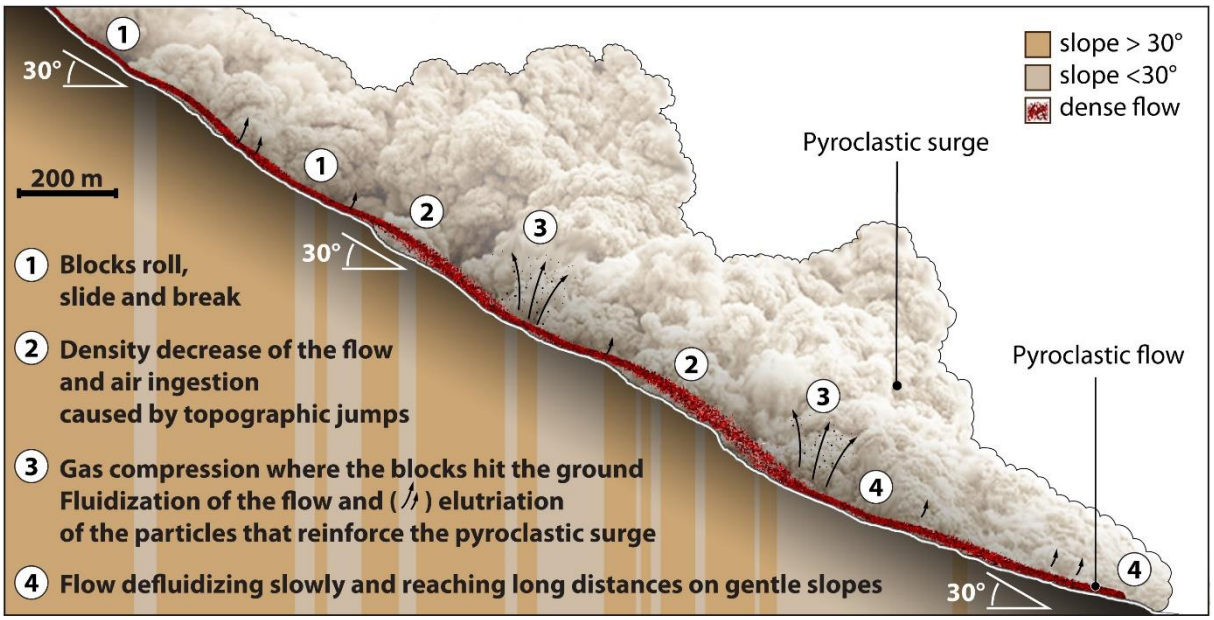

Figure 5. Mechanism of pyroclastic flow fluidization and genesis of pyroclastic surge by fluidization-elutriation cycles on the steeper volcanic slopes.

After its creation on steep slopes, the fluidity of the flow and its runout depends on two parameters: the gas diffusivity of the flow, related to the amount of fine particles, and the thickness of the flow. A thin flow, or a flow of coarse particles, cannot maintain the gas pressure needed to reach a long runout. The distance down which the bounces occur on the steepest slopes, which creates rocks comminution, abrasion and entrainment of previously deposited ash, thus favors long runouts.

Our model does not exclude the previously invoked models and many phenomena must occur simultaneously in the complex physics of PDCs. However, our cyclic fluidization-elutriation mechanism is so efficient experimentally that it can fully explain the genesis of very destructive pyroclastic surge and the long runout of dome collapse pyroclastic flows. The coherence between the experiments, the simulations and the field observations suggests that this model is a key mechanism for explaining PDC dynamics and it can help with future hazard predictions, by incorporating an accurate analysis of the volcano's topography.

Acknowledgements

The field observations were funded by the Domerapi ANR Project (ANR-12-BS06-0012), the OPGC, the LabEx ClerVolc (publication number 523), the IRD, the Merapi Observatory (BPPTKG/CVGHM) and the Instrumented Site VELI (IRD). We thank the two reviewers for their relevant comments.

Open Research

Numerical codes used for the block modeling and fluidized flow simulations are available at: https://doi.org/10.25519/1BSD-9R57

Images of the Merapi's activity (2014-2022) are available at: http://opgc.fr/SO/televolc/stereovolc/data/domerapi/Merapi.html

References

Bonnadona, C., Ernst, G. G. J. & Sparks, R. S. J. (1998).Thickness variations and volume estimates of tephra fall deposits: the importance of particle Reynolds number. *J. Volcanol. Geotherm. Res.*, **81**, 173–187

Branney, M. J. & Kokelaar, P. (2002). *Pyroclastic density currents and the sedimentation of ignimbrites*. *Geological Society Memoir No. 27*. doi:10.1086/427850.

Breard, E.C.P., Lube, G., Jones, J.R., Dufek, J., Cronin, S.J., Valentine, G.A. & Moebis, A. (2016). Coupling of turbulent and non-turbulent flow regimes within pyroclastic density currents. *Nat. Geosci.* **9**, 767–771

Breard, E. C. P. & Lube, G. (2017). Inside pyroclastic density currents – uncovering the enigmatic flow structure and transport behaviour in large-scale experiments. *Earth Planet. Sci. Lett.* **458**, 22–36

Breard, E. C. P., Dufek, J. & Lube, G. (2018). Enhanced Mobility in Concentrated Pyroclastic Density Currents: An Examination of a Self-Fluidization Mechanism. *Geophys. Res. Lett.* **45**, 654–664

Burgisser, A. & Bergantz, G. W. (2002). Reconciling pyroclastic flow and surge: The multiphase physics of pyroclastic density currents. *Earth Planet. Sci. Lett.* **202**, 405–418

Charbonnier, S. J. & Gertisser, R. (2008). Field observations and surface characteristics of pristine block-and-ash flow deposits from the 2006 eruption of Merapi Volcano, Java, Indonesia. *J. Volcanol. Geotherm. Res.* **177**, 971–982

Charbonnier, S. J, Germa, A., Connor, C.B., Gertisser, R., Preece, K., Komorowski, J.C., Lavigne, F., Dixon, T., Connora, L. (2013). Evaluation of the impact of the 2010 pyroclastic density currents at Merapi volcano from high-resolution satellite imagery, field investigations and numerical simulations. *J. Volcanol. Geotherm. Res.* **261**, 295–315

Chedeville, C. & Roche, O. Autofluidization of pyroclastic flows propagating on rough substrates as shown by laboratory experiments. *J. Geophys. Res. Solid Earth* **119**, 1764–1776 (2014).

Chedeville, C. & Roche, O. (2018). Autofluidization of collapsing bed of fine particles: Implications for the emplacement of pyroclastic flows. *J. Volcanol. Geotherm. Res.* **368**, 91–99

Cronin, S. J., Lube G., Dayudi, D.S., Sumarti, S., Subrandiyo S. & Surono (2013). Insights into the October-November 2010 Gunung Merapi eruption (Central Java, Indonesia) from the stratigraphy, volume and characteristics of its pyroclastic deposits. *J. Volcanol. Geotherm. Res.* **261**, 244–259

De'Michieli Vitturi, M., Esposti Ongaro, T., Lari, G. & Aravena, A. (2019). IMEX-SfloW2D 1.0: A depth-averaged numerical flow model for pyroclastic avalanches. *Geosci. Model Dev.* **12**, 581–595

Denlinger, R. P. (1987). A model for generation of ash clouds by pyroclastic flows, with application to the 1980 eruptions at Mount St. Helens, Washington. *J. Geophys. Res. Solid Earth* **92**, 10284–10298

Druitt, T. H. (1995). Settling behaviour of concentrated dispersions and some volcanological applications. *J. Volcanol. Geotherm. Res.* **65**, 27–39

Druitt, T. H. (1998). Pyroclastic density currents. *Geol. Soc. London, Spec. Publ.* **145**, 145–182

Druitt, T. H., Avard, G., Bruni, G., Lettieri, P. & Maez, F. (2007). Gas retention in fine-grained pyroclastic flow materials at high temperatures. *Bull. Volcanol.* **69**, 881–901

Dufek, J. (2016). The Fluid Mechanics of Pyroclastic Density Currents. *Annu. Rev. Fluid Mech.* **48**, 459–485

Esposti Ongaro, T., Clarke, A. B., Voight, B., Neri, A. & Widiwijayanti, C. (2012). Multiphase flow dynamics of pyroclastic density currents during the May 18, 1980 lateral blast of Mount St. Helens. *J. Geophys. Res. Solid Earth* **117**, B06208

Fries, A., Roche, O. & Carazzo, G. (2021). Granular mixture deflation and generation of pore fluid pressure at the impact zone of a pyroclastic fountain: Experimental insights. *J. Volcanol. Geotherm. Res.* **414**, 107226

Fujii, T. & Nakada, S. (1999). The 15 September 1991 pyroclastic flows at Unzen Volcano (Japan): A flow model for associated ash-cloud surges. *J. Volcanol. Geotherm. Res*. **89**, 159–172

Gueugneau, V., Kelfoun, K., Roche, O. & Chupin, L. (2017). Effects of pore pressure in pyroclastic flows: Numerical simulation and experimental validation. *Geophys. Res. Lett.* **44**, 2194–2202

Gueugneau, V., Charbonnier, S., Esposti Ongaro, T., de' Michieli Vitturi, M., Peruzzetto, M., Mangeney, A., Patra, A, Kelfoun, K. (2021). Synthetic benchmarking of concentrated pyroclastic current models. *Bull. Volcanol.* **83**, 1–32

Hungr, O. and Evans, S. G. (1996). Rock avalanche runout prediction using a dynamic model Proc. of the 7th Int. Symp. on Landslides (Norway, Trondheim) (Rotterdam: Balkema) Vol. 1 pp. 233-238

Kelfoun, K., Legros, F. & Gourgaud, A. (2000). A statistical study of trees damaged by the 22 November 1994 eruption of Merapi volcano (Java, Indonesia): Relationships between ash-cloud surges and block-and-ash flows. *J. Volcanol. Geotherm. Res.* **100**, 379–393

Kelfoun, K. & Druitt, T. H. (2005). Numerical modeling of the emplacement of Socompa rock avalanche, Chile. *J. Geophys. Res. Solid Earth* **110**, 1–13

Kelfoun, K., Santoso, A.B., Latchimy, T. *et al.* (2021). Growth and collapse of the 2018–2019 lava dome of Merapi volcano. *Bull. Volcanol.* **83**, 8

Komorowski, J. C., Jenkins, S., Baxter P. J. *et al.* Paroxysmal dome explosion during the Merapi 2010 eruption: Processes and facies relationships of associated high-energy pyroclastic density currents. *J. Volcanol. Geotherm. Res.* **261**, 260–294 (2013).

Lube, G., Cronin, S. J., Thouret, J.-C. & Surono (2011) Kinematic characteristics of pyroclastic density currents at Merapi and controls on their avulsion from natural and engineered channels. *Geol. Soc. Am. Bull.* **123**, 1127-1140

Lube, G., Breard, E. C. P., Cronin, S. J. & Jones, J. (2015). Synthesizing large-scale pyroclastic flows: Experimental design, scaling, and first results from PELE. *J. Geophys. Res. Solid Earth* **120**, 1487–1502

Lube, G., *Breard, E. C. P., Jones J., Fullard L., Dufek J., Cronin S. J. & Wang T.* (2019). Generation of air lubrication within pyroclastic density currents. *Nat. Geosci.* **12**, 381–386

Lube, G., Breard, E. C. P., Esposti-Ongaro, T., Dufek, J. & Brand, B. (2020). Multiphase flow behaviour and hazard prediction of pyroclastic density currents. *Nat. Rev. Earth Environ.* **1**, 348–365

Matsusaka, S., Kobayakawa, M., Mizutani, M., Imran, M. & Yasuda M., (2013). Bubbling behavior of a fluidized bed of fine particles caused by vibration-induced air inflow. *Sci. Rep.* **3**, 1190

McTaggart, K. C. (1960). The mobility of nuées ardentes. *Amer. J. Sci.* **258**, 369

Montserrat, S., Tamburrino, A., Roche, O. & Niño, Y. (2012). Pore fluid pressure diffusion in defluidizing granular columns. *J. Geophys. Res. Earth Surf.* **117**, 1–15

Montserrat, S., Tamburrino, a., Roche, O., Niño, Y. & Ihle, C. F. (2016). Enhanced run-out of dam-break granular flows caused by initial fluidization and initial material expansion. *Granul. Matter*

Nakada, S. & Fujii, T. (1993). Preliminary report on the activity at Unzen Volcano (Japan), November 1990-November 1991: Dacite lava domes and pyroclastic flows. *J. Volcanol. Geotherm. Res.* **54**, 319–333

Pak, H. K. & Behringer, P. R. (1994). Bubbling in vertically vibrated granular materials. *Nature* **371**, 231–233

Patra, A., Bevilacqua A., Akhavan-Safaei A., Pitman E. B., Bursik M., Hyman D. (2020). Comparative Analysis of the Structures and Outcomes of Geophysical Flow Models and Modeling Assumptions Using Uncertainty Quantification. *Front. Earth Sci.* **8**

Peruzzetto, M., Mangeney, A., Bouchut, F., Grandjean, G., Levy G., et al. (2020). Topography curvature effects in thin-layer models for gravity-driven flows without bed erosion. *J. Geophys. Res.: Earth Surface*, 126 (4)

Roche, O. (2012). Depositional processes and gas pore pressure in pyroclastic flows: an experimental perspective. *Bull. Volcanol.* **74**, 1807–1820.

Sato, H., Fujii, T. & Nakada, S. (1992). Crumbling of dacite dome lava and generation of pyroclastic flows at Unzen volcano. *Nature* **360**, 664–666

Sparks, R. S. J. (1976). Grain size variations in ignimbrites and implications for the transport of pyroclastic flows. *Sedimentology* **23**, 147–188

Sparks, R.S.J. & Wilson, L. (1976). A model for the formation of ignimbrite by gravitational column collapse. *J. Geol. Soc. London*. **132**, 441—451

Sparks, R. S. J., Wilson, L. & Hulme, G. (1978). Theoretical Modeling of the generation, movement,and emplacement of pyroclastic flows by column collapse. *J. Geophys. Res.* **83**, 1727–1739

Sparks, R., Bursik, M., Carey, S., Gilbert, J., Glaze, L., Sigurdsson, H. & Woods, A. (1997). Volcanic Plumes. Wiley, New Jersey

Sweeney, M. & Valentine, G. (2017). Impact zone dynamics of dilute mono- and polydisperse jets and their implications for the initial conditions of pyroclastic density currents. *Physics of Fluids*. **29** (9), 093304

Valentine, G. A. & Sweeney, M. R. (2018). Compressible Flow Phenomena at Inception of Lateral Density Currents Fed by Collapsing Gas-Particle Mixtures. *J. Geophys. Res. Solid Earth* **123**, 1286–1302

Valentine, G. A. (2020). Initiation of dilute and concentrated pyroclastic currents from collapsing mixtures and origin of their proximal deposits. *Bull. Volcanol.* **82**

Wilson, C. J. N. (1980). The role of fluidization in the emplacement of pyroclastic flows: An experimental approach. *J. Volcanol. Geotherm. Res.* **8**, 231–249

Zamankhan, P. (2012). Solid structures in a highly agitated bed of granular materials. *Appl. Math. Model.* **36**, 414–429